Supplementary Information

Defective Wnt-dependent cerebellar midline fusion in a mouse model of Joubert syndrome

Madeline A. Lancaster, Dipika J. Gopal, Joon Kim, Sahar N. Saleem, Jennifer L. Silhavy, Carrie M. Louie, Bryan E. Thacker, Yuko Williams, Maha S. Zaki, Joseph G. Gleeson

Supplemental Figure 1

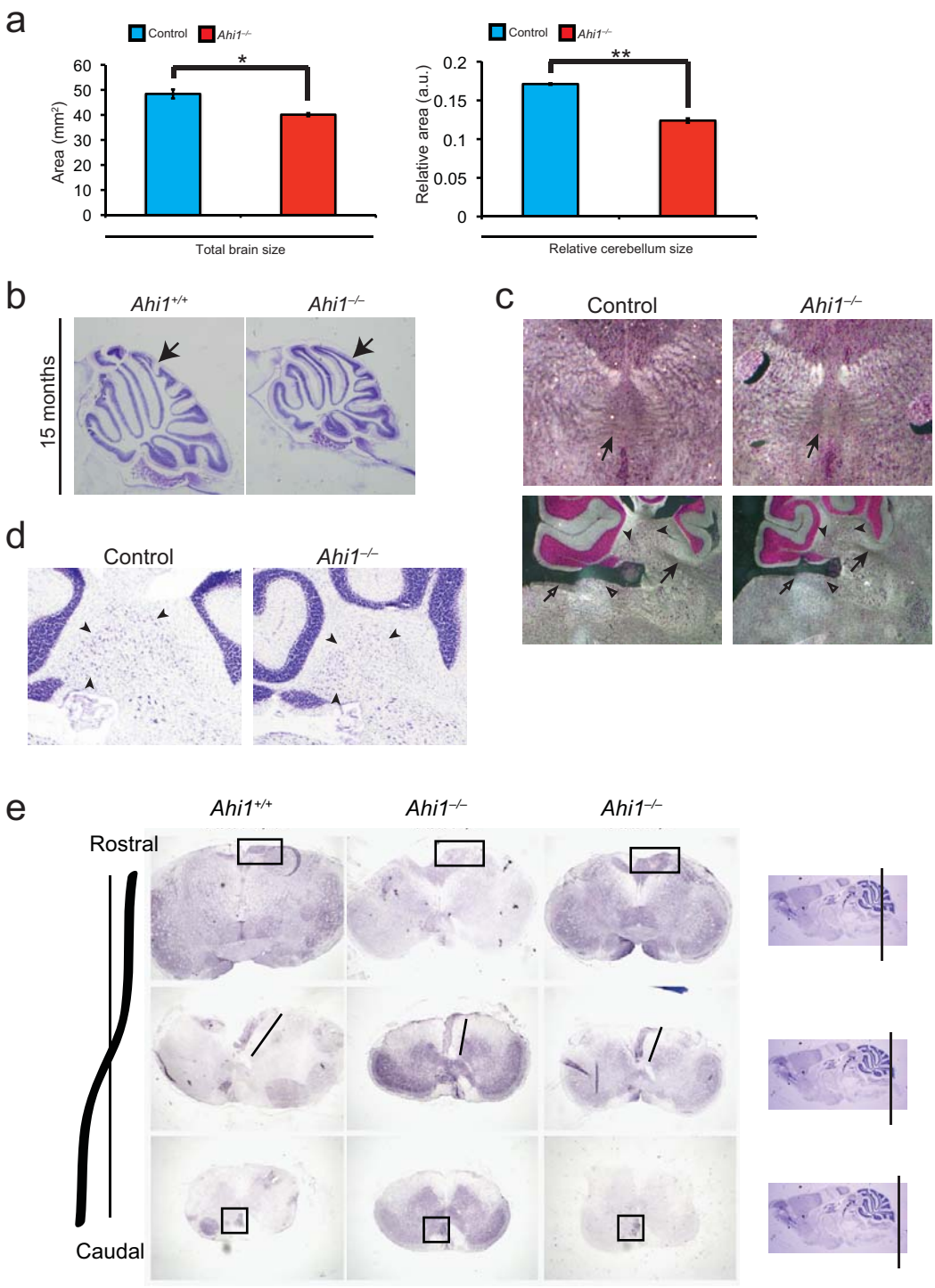

Supplemental Figure 1. Later phenotype but intact brainstem structures. a. Average total brain area size measurements for *Ahi1* mutants compared with littermate controls (left). Average cerebellum area size relative to total brain area (a.u.=arbitrary units) from *Ahi1* mutants compared with littermate controls (right). *P<0.05, **P<0.0005 Student's t-test, n=3 for each genotype. b. Representative 15 month old littermate sagittal C-V stained sections revealing persistent size and foliation defects (arrows). c. Top, C-V stained coronal sections revealing intact superior cerebellar peduncles (arrow) in *Ahi1*$^{-/-}$ compared with littermate control. Bottom, C-V stained mediolateral sagittal sections revealing intact brainstem structures in *Ahi1* mutants. Arrowheads=deep cerebellar nuclei, arrow=superior cerebellar peduncle, open arrows=descending trigeminal tract, open arrowheads=dorsal column nuclei. d. C-V stained sagittal paramedical sections of cerebella from *Ahi1* mutant and control littermate at higher magnification revealing deep cerebellar nuclei (arrowheads). e. Biotinylated dextran amine (BDA) tracing assay in two *Ahi1* mutants and littermate control. Coronal sections through brainstem and spinal cord reveal crossing of pyramidal axons from rostral to caudal sections. Boxes outline DAB positive axons and lines reveal crossing of axons.

Supplemental Figure 2

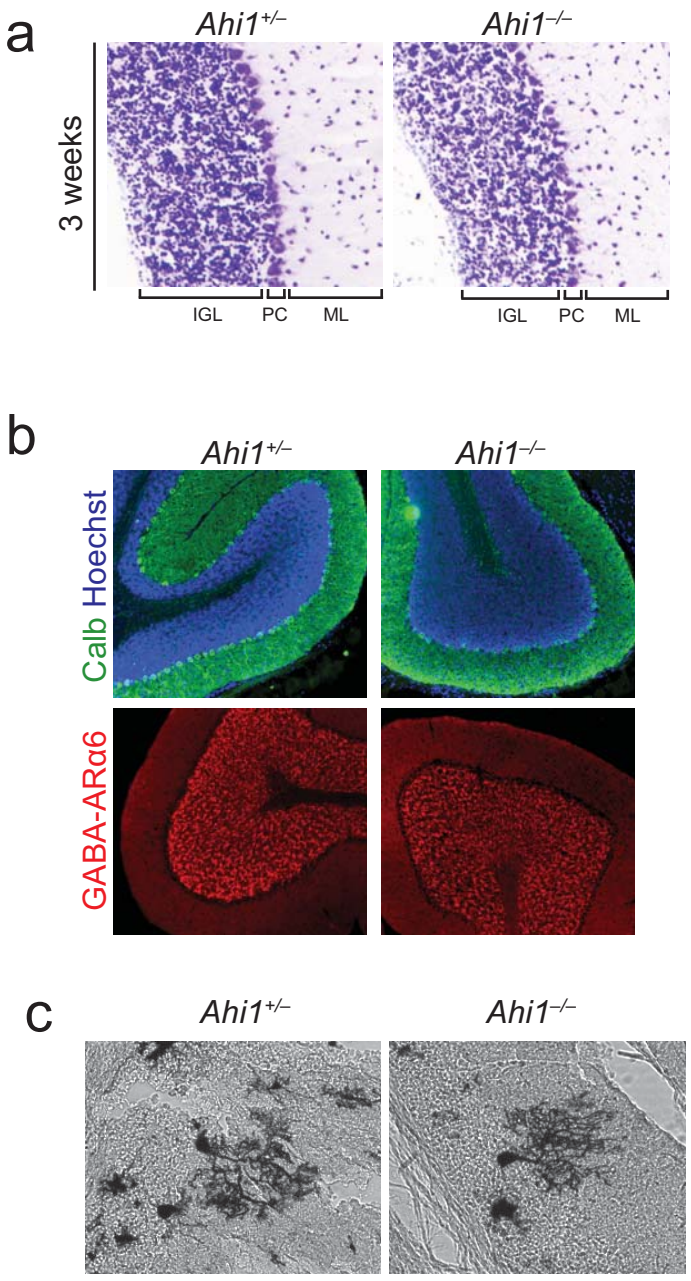

Supplemental Figure 2. Normal layering in *Ahi1* mutant cerebella. a. High magnification image of layering within the cerebellar vermis of *Ahi1* mutant and littermate control as visualized by C-V staining of sagittal sections. Layers are shown: inner granule layer (IGL), Purkinje cell layer (PC), molecular layer (ML). b. Staining for cerebellar layers appears intact in *Ahi1* mutants. Calbindin (green) labels Purkinje neurons, GABA-A receptor α6 (GABA-ARα6, red) labels inner granule layer. Hoechst (blue) labels nuclei. c. Golgi-Cox staining revealing dendritic tree architecture of Purkinje neurons in $Ahi1^{-/-}$ and $Ahi1^{+/-}$ cerebella.

Supplemental Figure 3

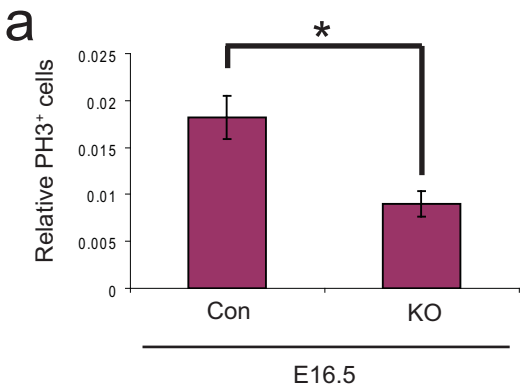

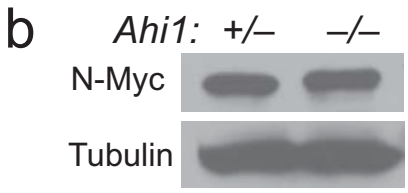

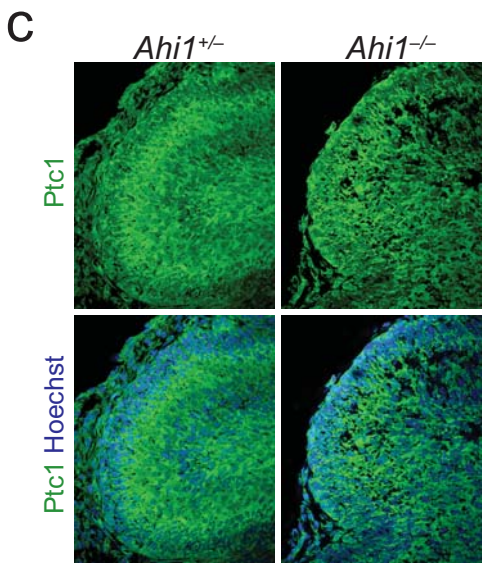

Supplemental Figure 3. Early proliferation defects but intact Shh signaling in *Ahi1* mutants. a. Average number of phospho-histone H3 (PH3) stained external granule layer neurons (EGL) at E16.5 relative to total cells in EGL. *P<0.05, Student's t-test, n=3. b. Western blot on whole cerebellum lysates from P5 littermates. N-myc antibody recognizes a primary band at approximately 70kDa. Tubulin is the loading control. c. Ptc1 (green) staining in P5 midline sagittal sections from *Ahi1*$^{-/-}$ and *Ahi1*$^{+/-}$ littermates. Hoechst (blue) labels nuclei.

Supplemental Figure 4

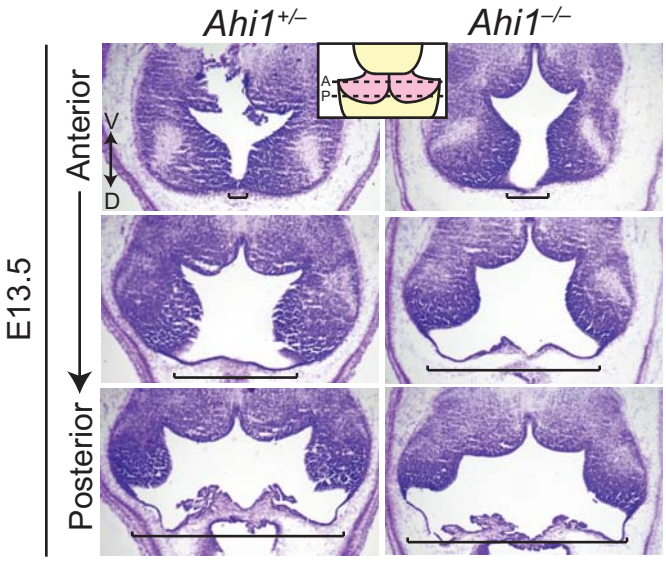

Supplemental Figure 4. Roof plate widening in *Ahi1* mutants. Matched transverse C-V stained sections from littermates arranged in a series from anterior to posterior revealing the progressive posterior widening of the roof plate in *Ahi1* mutant (bars). Diagram inset depicts approximate locations of anterior and posterior sections.

Supplemental Figure 5

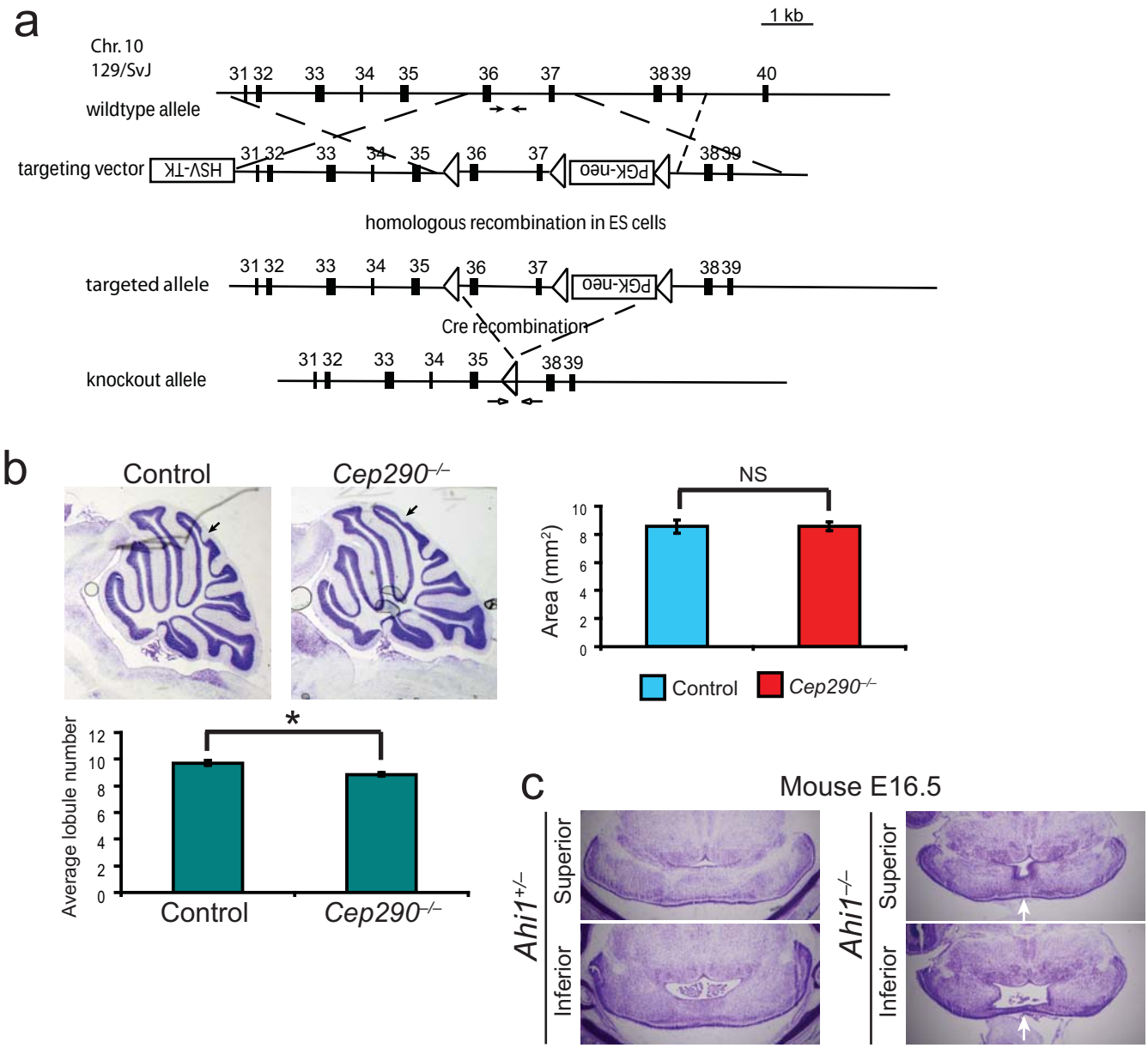

Supplemental Figure 5. *Cep290* targeting and adult phenotype. a. Schematic of targeting approach used to generate *Cep290* null mice described in methods. Homologous recombination is represented by dashed crossing lines, and resulting alleles are shown. Positions for genotyping primers are shown: Closed arrows are wild-type primers, open arrows are knock-out primers. b. Left, representative midline sagittal C-V stained sections from adult *Cep290*$^{-/-}$ and littermate control. Arrow points to mild foliation defect in *Cep290* mutants. Right, quantification of average vermis area in *Cep290*$^{-/-}$ and littermate controls. NS=not significant, Student's t-test, n=3 for each genotype. Bottom, quantification of average number of lobules in *Cep290*$^{-/-}$ littermate controls. *P<0.05, Student's t-test, n=3 for each genotype. Error bars are S.E.M. c. Transverse C-V stained sections from *Ahi1* mutant and littermate control shown in series from superior to inferior. Arrow points to fusion defect.

Supplemental Figure 6

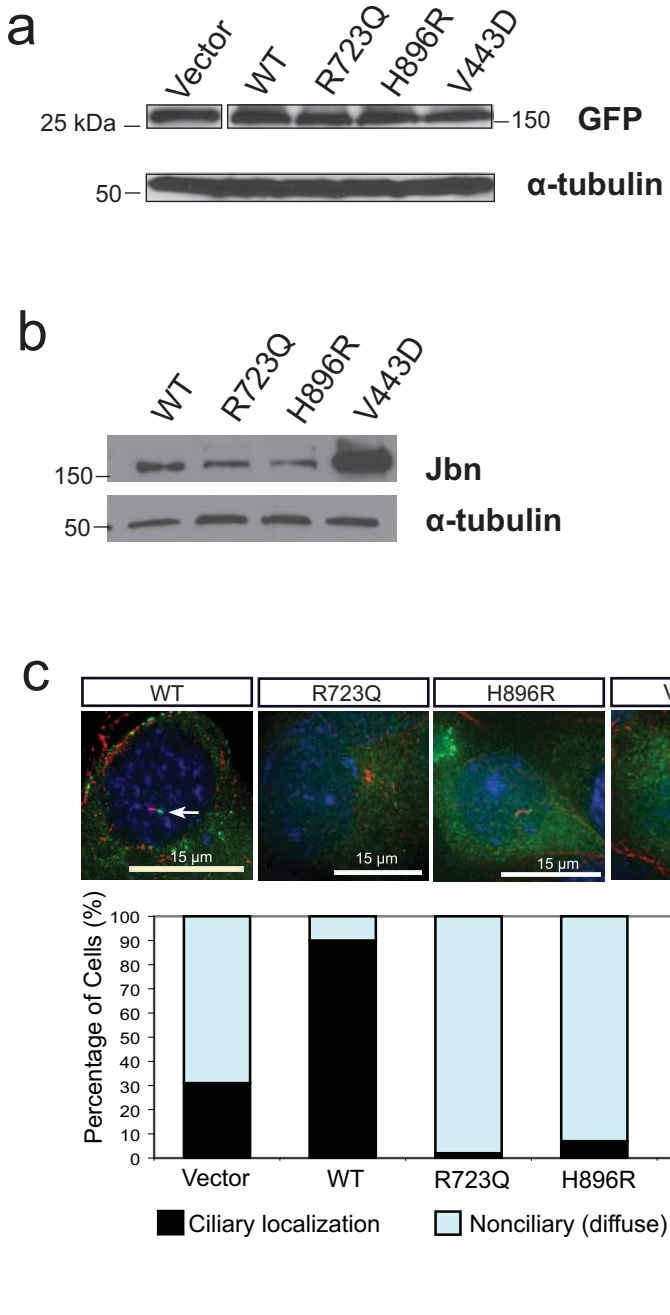

Supplemental Figure 6. Expression analysis and localization of disease mutations. a. Western blot from 293T cells transfected with mutant constructs and assayed for GFP levels. Tubulin represents the loading control. b. Western blot from IMCD cells transfected with mutant constructs and assayed for Jbn levels. Tubulin represents the loading control. c. Localization of Jbn disease mutation constructs (green) in IMCD cells stained for cilia (acetylated tubulin, red). Hoechst labels nuclei. Below, quantification of cilia localization in 100 cells for each construct.

Supplemental Figure 7

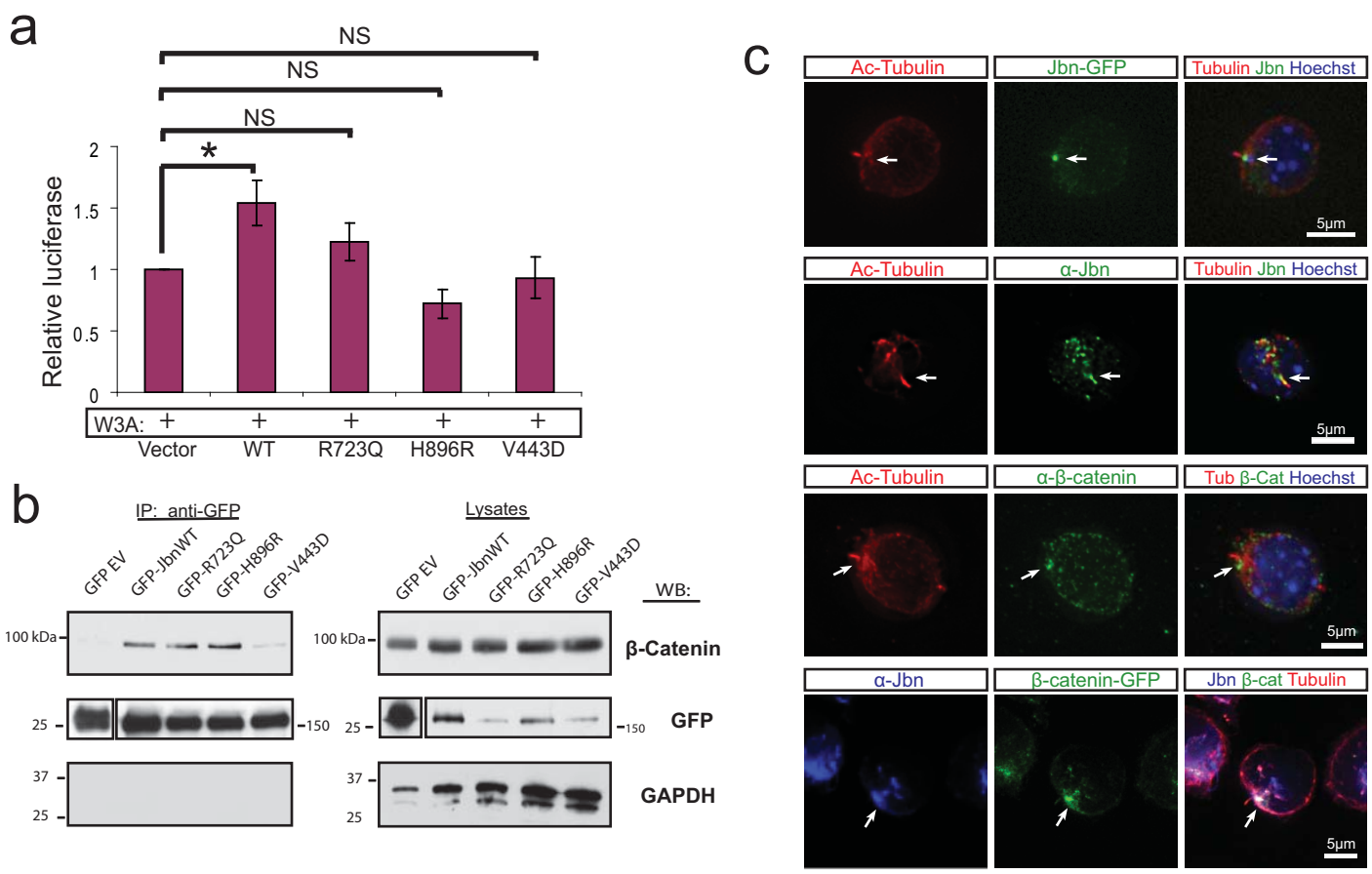

Supplemental Figure 7. Disease mutations fail to potentiate Wnt signaling. a. Luciferase activity in fibroblasts transfected with wild-type Jbn or mutant constructs and treated with Wnt3A (W3A) conditioned media. NS=not significant, *P<0.05, Student's t-test, n=3. Error bars are S.E.M. b. Co-immunoprecipitation in 293T cells of Jbn GFP constructs pulled down with GFP antibody and western blot for endogenous β-catenin which reveals interaction between β-catenin and wild-type Jbn as well R723Q and H896R but not with V443D. GFP western blot reveals efficiency of immunoprecipitation, while GAPDH is a negative control. c. Localization of Jbn-GFP construct (green, first row) or endogenous Jbn (green, second row) to cilia (arrows) stained for acetylated tubulin (red) in CGNs isolated from wild-type P5 cerebella. Ciliary localization of endogenous β-catenin (green, third row) and colocalization of β-catenin-GFP construct (green, fourth row) with endogenous Jbn (blue) at the cilium (acetylated tubulin, red). Hoechst (blue) labels nuclei in the first three rows.

Supplemental Figure 8

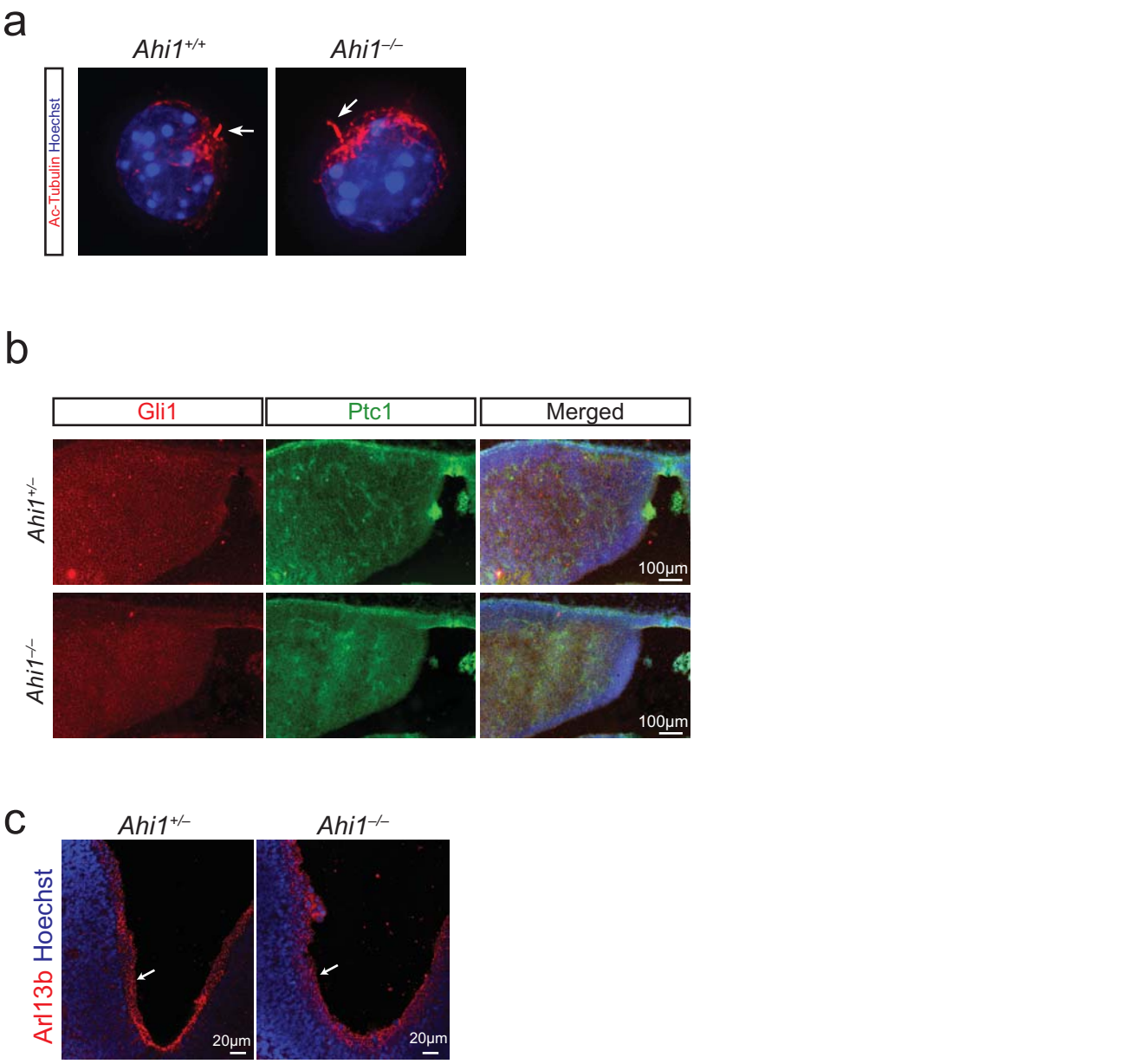

Supplemental Figure 8. Cilia staining in *Ahi1* mutant cerebellar neurons. a. Cilia staining (arrows, acetylated tubulin, red) in isolated CGNs from P5 littermates. Hoechst labels nuclei (blue). b. Shh target gene staining in E14.5 transverse sections from *Ahi1*$^{-/-}$ and *Ahi1*$^{+/-}$ littermates. Gli1 (red) is not expressed at this stage. Ptc1 (green) is also weakly expressed primarily in the future EGL as well as at the site of fusion. This expression appears equally low in the *Ahi1* mutant. Hoechst (blue) labels nuclei. c. Arl13b staining (red) to visualize cilia (arrows) on transverse sections of *Ahi1*$^{-/-}$ and littermate control cerebella at E13.5. Hoechst (blue) labels nuclei.

Supplemental Figure 9

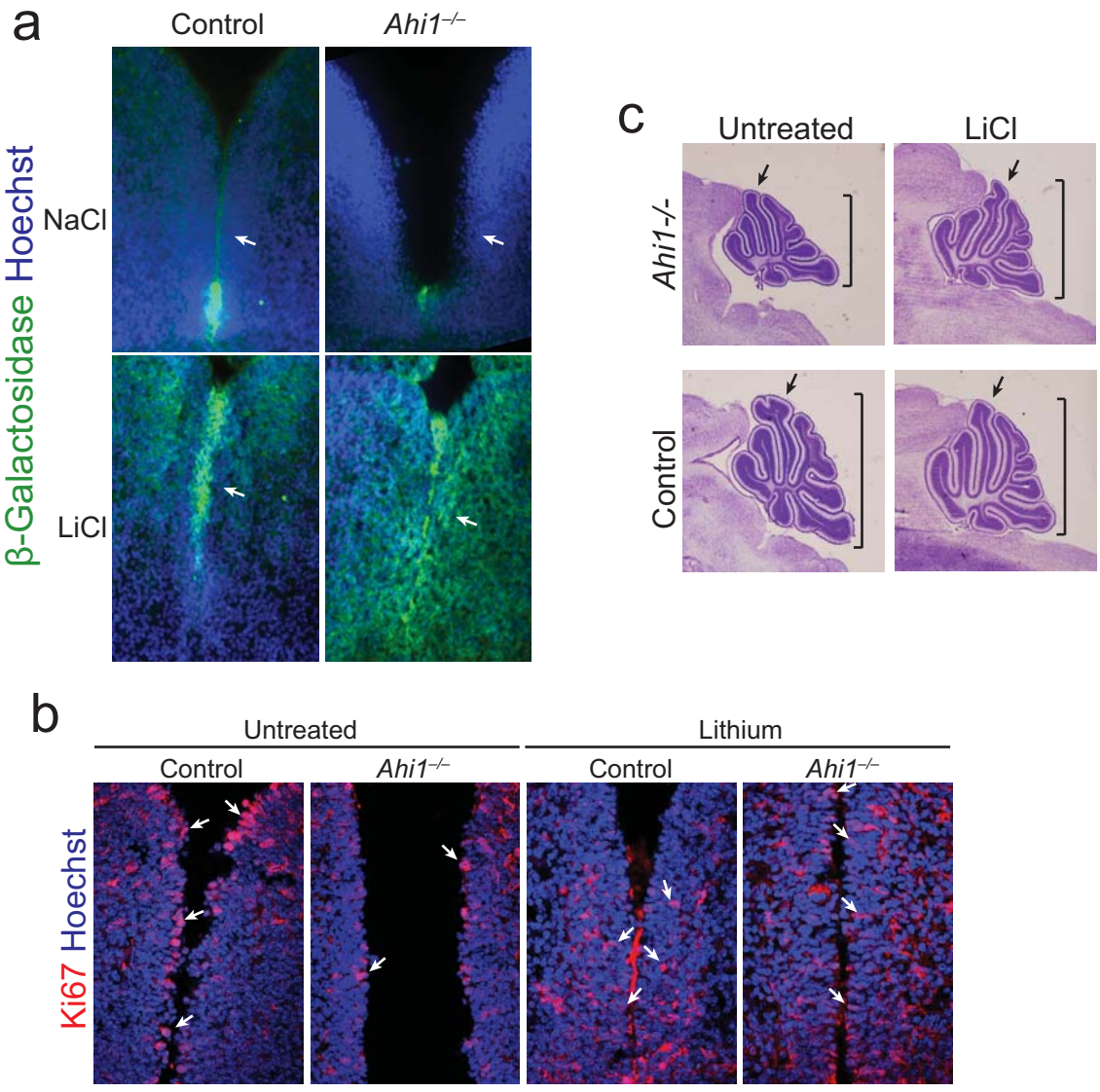

Supplemental Figure 9. Wnt activity staining in LiCl treated embryos. a. β-galactosidase (green) staining of transverse sections from E14.5 BATgal+ embryos treated with NaCl or LiCl reveals increased Wnt activity (arrows) with LiCl treatment in both control and *Ahi1*$^{-/-}$ embryos compared with NaCl treated embryos. Hoechst (blue) labels nuclei. b. Ki67 staining (red, arrows) in *Ahi1*$^{-/-}$ and *Ahi1*$^{+/-}$ littermate controls treated with LiCl compared with untreated controls which was quantified in Figure 4f. Hoechst labels nuclei. c. Cresyl-violet sagittal sections from P11 littermates treated with LiCl at E12.5 and E13.5 or untreated.

Supplemental Figure 10

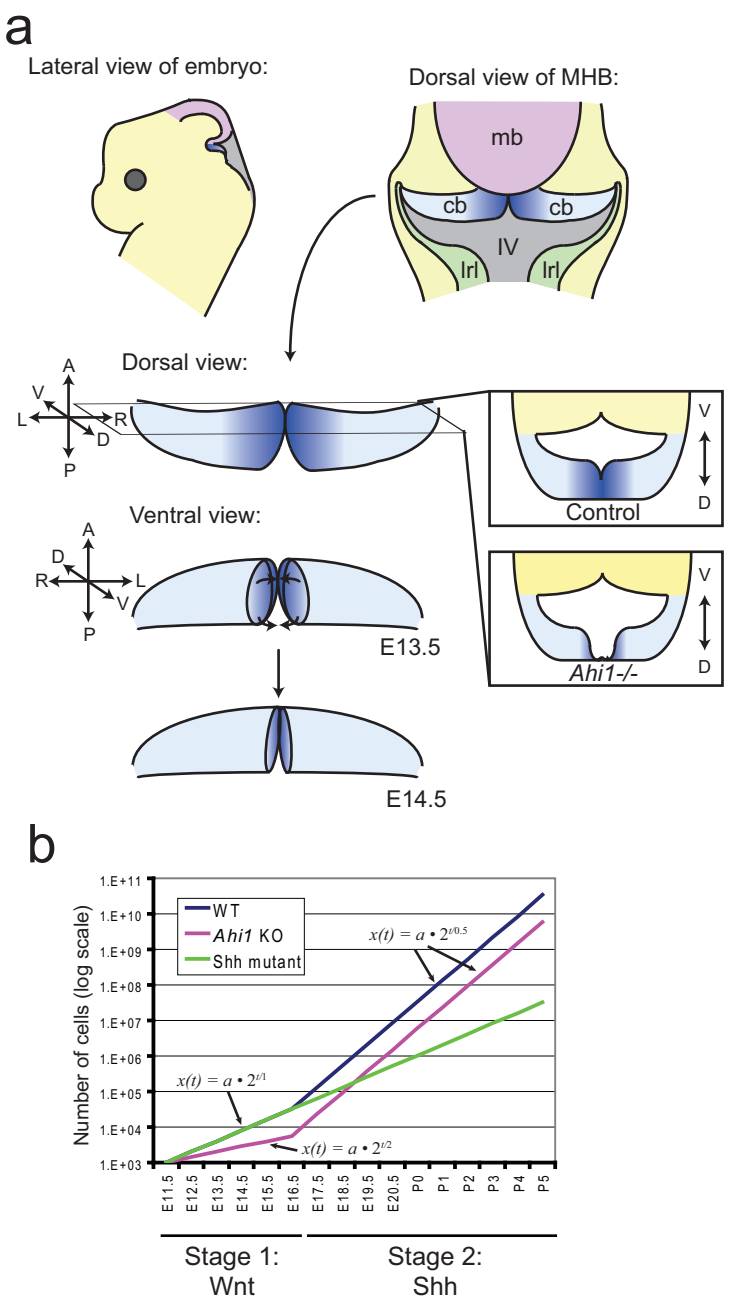

Supplemental Figure 10. Fusion model and mathematical modeling of a two stage proliferation model. a. Model of midline cerebellar fusion and its disruption in *Ahi1* mutant mice. The embryonic head is shown from the side and a close up view of the mid-hindbrain junction (MHB) is shown from the dorsal surface revealing the midbrain (mb), cerebellar hemispheres (cb), lower rhombic lip (lrl) and fourth ventricle (IV). A dorsal view of the isolated cerebellum is shown with a depiction of the plane of sectioning for transverse sections (shown in a schematic at the right) and axes at the left: anterior (A), posterior (P), left (L), right (R), ventral (V), dorsal (D). The ventral view of the fusing cerebellum reveals the fusion events that occur and are visible on transverse sections. A progression from E13.5 to E14.5 is depicted to provide a sense of the closure that occurs. b. Mathematical modeling of the proliferation defect in *Ahi1* knock-out (KO) mice compared with wild-type and a hypothetical Shh mutant. Equations are shown for each segment. See supplemental text.